JOURNAL OF CATALYSIS 140, 481–496 (1993)

Hydrocarbon-Induced Agglomeration of Pd Particles in Pd/HZSM-5

ZONGCHAO ZHANG,[1] BRUCE LERNER, GUAN-DAO LEI, AND WOLFGANG M. H. SACHTLER[2]

V.N. Ipatieff Laboratory, Chemistry Department, Northwestern University, Evanston, Illinois 60208

Received July 6, 1992; revised October 23, 1992

The deactivation mechanism of Pd/HZSM-5 catalysts in the conversion of methylcyclopentane (MCP) has been studied. Results obtained with EXAFS and TEM show that agglomeration of Pd particles is the dominant cause of catalyst deactivation; no coke deposition is detected by TPO, ^{13}C-NMR, or TEM. In a freshly reduced 0.88-wt% Pd/HZSM-5 catalyst, triatomic Pd particles are stabilized by protons bridging between Pd_3 and the cage wall. During MCP reaction at 250°C the Pd_3 clusters coalesce, forming much larger Pd particles of about 20 Å. This agglomeration induces significant changes in the product distribution pattern of the isotope exchange between cyclopentane (CP) and D_2. The agglomeration is attributed to "de-anchoring," i.e., the replacement of the protons in Pd_n–H^+–O^- by carbenium ions. This concept is confirmed by exposing the reduced catalyst to NH_3: proton neutralization induces formation of 50-Å large Pd particles. Metal agglomeration is much smaller after exposure to CP instead of MCP; this evidence illustrates the crucial role of the tertiary C atom in MCP. It is concluded that the easy formation of a tertiary carbenium ion is essential for extensive deanchoring. The agglomerated Pd particles are still inside the zeolite for a low-Pd-loading catalyst, but for a catalyst with high Pd loading a significant portion of the secondary Pd particles are on the external surface. In this case the distribution of the isotope-exchange pattern of CP + D_2 becomes similar to that of Pd/SiO_2.

I. INTRODUCTION

Zeolites are capable of encapsulating small, catalytically active metal particles. This phenomenon is generally attributed to the geometric limitations imposed on the growth of metal particles by the dimensions of zeolite cages or channels. However, we recently showed that Pt and Pd metal particles as small as 1–6 atoms can be generated and stabilized in zeolite cages (*1*). As such metal clusters are smaller than the cage windows, geometric restrictions do not apply to their migration. We proposed a novel model, i.e., "proton anchoring," to explain the unusual stabilization of primary metal particles (*1*). Several sets of independent experimental data obtained in our lab substantiate this model. Protons are formed as charge-compensating cations during the reduction by H_2 of metal ions. These protons strongly interact with the reduced transition metal atoms or particles, while they are also bonded to oxide ions of the cage walls. The proton bridge between transition metal and cage wall is at the base of the anchoring phenomenon which stabilizes small metal particles. For zeolite-Y-supported Pd, rapid de-anchoring of the primary Pd particles takes place when the catalysts are exposed to CO at room temperature (*1*, *2*). This release of the proton anchors is detected by an increase in FTIR intensity of the band due to the zeolite OH groups (*3*). Carbonyl clusters are thus formed which coalesce with each other to the extent limited by the geometric restrictions of the apertures between cages. While $Pd_{13}(CO)_x$ prevails at room temperature in zeolite Y, (*1*, *2*), hexanuclear $Pd_6(CO)_y$ clusters are entrapped in zeolite 5A (*4*), the subscripts x and y depending on the CO partial pressure. The proton-anchoring model is confirmed by EXAFS data of the Pd particle size in HY

[1] Present address: Johnson Matthey, 456 Devon Park Drive, Wayne, PA 19087.

[2] To whom correspondence should be addressed.

0021-9517/93 $5.00

and NaHY (*5*). After calcination at 500°C and reduction by H_2 at 350°C, the average nearest Pd–Pd coordination number CN_{Pd} is 4 for Pd/NaHY, which can be interpreted as octahedral Pd_6 clusters, but for Pd/HY CN_{Pd} it is 2.4, corresponding to trigonal and tetrahedral Pd_3 and Pd_4. Although the Pd particles in Pd/HY are smaller than in Pd/NaHY, Pd/HY chemisorbs less hydrogen due to a higher x/n value of the $[Pd_n–H_x]^{x+}–O_x^-$ adducts. A recent XPS study suggests that the x-value increases with proton concentration (*6*).

Protons that bond directly to metal particles can significantly affect the catalytic performance of the metal. Electron-deficient proton adducts of Pt and Pd particles in zeolite Y have been found to be much more active in certain hydrocarbon reactions than the same metals in the absence of protons (*7*). In addition, the selectivity can be significantly altered by the participation of the protons. It is conceivable, that protons of the metal–proton adduct are chemically involved in the catalytic reaction. This leads to the question motivating the present study, how such involvement would affect the anchoring function of the same protons. If, e.g., a carbenium ion is formed by chemical interaction between a hydrocarbon molecule and a proton, bridging between a metal cluster and an oxide ion of the cage wall, this could reduce the anchoring effect for the metal cluster. The present work attempts to verify the validity of this concept. The conversion of methylcyclopentane (MCP) is used as a probe reaction over Pd/HZSM-5 catalysts. Cyclopentane (CP) is used in the characterization stage to elucidate the effect of carbon type in the reaction mechanism.

II. EXPERIMENTAL

IIa. Catalyst Preparation

A diluted solution of $Pd(NH_3)_4^{2+}$ ions (0.05 mol/1000 cm^3) was added dropwise into a slurry of NH_4ZSM-5 (5 g in 1000 cm^3 deionized distilled water). The ion exchange was performed for 24 h at room temperature. The Pd loadings, as determined by atomic absorption, are 0.88 and 3.5 wt%, respectively. The catalysts were then filtered and dried in air.

IIb. Methylcyclopentane Conversion

The catalysts (0.1000 g each) were calcined in O_2 flow (200 cm^3/min) at 500°C for 2 h after ramping at 0.5°C from room temperature. They were subsequently purged with He at 500°C for 20 min before being cooled to room temperature. Reduction with H_2 was carried out at a heating rate of 8°C/min from 21°C to 230°C and then at 1°C/min from 230 to 250°C. Samples were kept at 250°C for 20 min in H_2; then a flow of H_2 loaded with methylcyclopentane (MCP) by passing through an MCP reservoir held at 0°C was led over the catalysts. The H_2/MCP ratio was 16 and the total flow 20 cm^3/min. The effluent gases were analyzed by an on-line HP5794 gas chromatograph with a 50 m crosslinked methylsilicone fused capillary column and a FID detector. Conversions are used to depict catalyst activities; due to substantial changes of metal dispersion during reaction, use of turnover frequencies is not meaningful.

IIc. Temperature-Programmed Oxidation (TPO)

The TPO technique was applied to follow the coke oxidation products of used catalysts. TPO runs were carried out using an on-line Dycor M200 mass spectrometer downstream as a detector and an interfaced computer for data recording. A leaking valve was used for continuous sampling. The used catalysts were purged with He at room for 20 min after reaction. A mixture of 5% O_2/Ar was used with a flow of 60 cm^3/min. Each TPO experiment was started at 20°C and was stopped at 550°C using a programmed heating rate of 8°C/min.

IId. Nuclear Magnetic Resonance (NMR)

^{13}C-NMR spectroscopy was applied to determine the type of coke in the used catalysts. A used Pd/HZSM-5 (0.88 wt% Pd) was loaded into a boron nitride rotor in a

glovebox under N_2 atmosphere from a sealed reactor. The rotor was immediately loaded into a probe that was kept at N_2 atmosphere during measurement. ^{13}C-NMR experiments were performed at 75.4 MHz on a VXR-300 solid-state NMR spectrometer at room temperature. Cross-polarization and magic-angle-spinning (CP-MAS) are used with a spin rate of 6.7 kHz, a 90° pulse of 4.5 μs for ^{13}C and a 90° pulse of 17.5 μs for ^{1}H. The contact time was 2.5 μs. Data acquisition took about 3 h.

IIe. Cyclopentane H/D Exchange

Exchange of the H atoms in cyclopentane (CP) with D_2 is used as a qualitative probe for the accessibility of Pd particles in HZSM-5 pores and for the sites catalyzing this exchange. Exchange measurement were performed in a recirculation flow system as described previously (*8*). The isotope exchange was monitored by a mass spectrometer (Dycor M100) with a variable leak valve from the reaction system. All samples were reduced in a flow of D_2 prior to H/D exchange. The exchange reactions were carried out at 100°C with a molar ratio D_2/CP of 25/1 and a total pressure of 52 Torr. The initial product distribution (at leas than 10% conversion) was calculated according to the method of van Broekhoven and Ponec (*9*). The initial rate for the disappearance of CP $[-d(d_0)/dt]$ was calculated by standard means (*10*) and was corrected for physisorption of CP in zeolite. The d_i fraction is defined as the ratio of the deutero-CP molecules with i D atoms to the total number of all CP molecules. Samples were probed after exposure for 1 h to D_2/CP or D_2/MCP gas mixtures at 250°C. After each exposure to such a mixture, the reaction vessel was evacuated for 1 h at 250°C until no more hydrocarbons were detected by the mass spectrometer.

IIf. Extended X-ray Absorption Fine Structure (EXAFS) Spectroscopy

EXAFS spectroscopy was used to determine the Pd particle size for a Pd/HZSM-5 sample with Pd loading of 0.88 wt%. This technique is particularly useful to determine particle sizes below the detection limit of HRTEM of XRD. After reduction at 250°C in H_2 for 40 min and purging at the same temperature with He for 20 min, a sample is sealed in a glass reactor; subsequent pellet formation and transfer into an EXAFS holder is done in a glovebox. Half of the same batch is used as a catalyst in MCP conversion for 1 h at the conditions specified above. After use, the catalyst is prepared for characterization by EXAFS in the same fashion as the fresh catalyst. The total time that the catalyst was maintained at 250°C in H_2 and He was equal to that during which the catalyst was exposed to MCP.

EXAFS data collection at the Pd *K*-edge was performed in transmission mode at CHESS. A typical beam energy is 5.2 GeV and the beam current is 70–90 mA. A stainless EXAFS cell was used in the transmission mode, as described previously (*1*). During data collection samples were kept at 90 K. A Pd foil of 0.025 mm and PdO powder were used as reference structures for EXAFS data analysis. The coordination number (CN) of Pd in the reference foil is taken as 12, and the nearest neighbor Pd–Pd bond distance R_{Pd-Pd} in the foil is 2.75 Å. The Debye–Waller factor for the Pd foil is 0.011 Å. The CN in PdO reference is assigned to 4 and R_{Pd-O} to 2.01 Å. The Debye–Waller factor for PdO is 0.005 Å.

IIg. Transmission Electron Microscopy (TEM)

Electron micrographs were taken using a Hitachi HF-2000 High-Resolution Analytical Electron Microscope (HRAEM) equipped with a field emission gun electron source. The instrument is operated at a 200 kV accelerating voltage. Magnification of 10^5 in conjunction with a suitable aperture permits imaging without large scale beam damage to the susceptible zeolite. Samples are prepared as powders dispersed on holey carbon grids or are embedded in a hard resin and microtomed with a glass knife. Thin sections

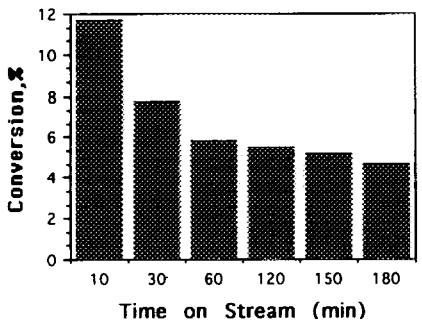

FIG. 1. Deactivation pattern of 3.5-wt% Pd/HZSM-5 in MCP conversion.

in the "gold region" (ca. 90 nm) are supported on holey carbon grids or sandwiched between 200–300 mesh folding grids to eliminate sample drift in the electron beam.

Four samples were examined by TEM: (1) freshly reduced Pd/HZSM-5 (0.88-wt% Pd) at 250°C (40 min in H_2 and 20 min in He); (2) same after MCP conversion at 250°C for 1 h; (3) after CP conversion at 250°C for 1 h; and (4) a sample reduced in pure H_2 at 250°C as sample (1), but subjected to a flow (60 cm^3/min) of a 3/1 H_2/NH_3 mixture.

III. RESULTS

IIIa. MCP Conversion

In the present paper, we mainly focus on the catalyst deactivation and Pd agglomeration in HZSM-5. Observed changes in selectivity of converting MCP to the ring-opening products (*n*-hexane, 2- and 3-methylpentane) and the ring-enlargement products (benzene and cyclohexane) will be discussed elsewhere. In brief, *n*-hexane selectivity and the 2-MP/3-MP ratio increase dramatically, corresponding to the growth of Pd nuclearity with time on stream. In the extreme case, the 2-MP/3-MP ratio approaches 4. Figures 1 and 2 show the conversion as a function of time on stream (TOS) for catalysts with Pd loading of 3.5 and 0.88 wt%, respectively. Deactivation is rapid for the first 60 min but slower afterward. Cyclopentane is chosen in a treatment of a freshly reduced catalyst for the purpose of investigating its effect on Pd particle agglomeration; no attempt was made to follow its catalyzed conversion in detail.

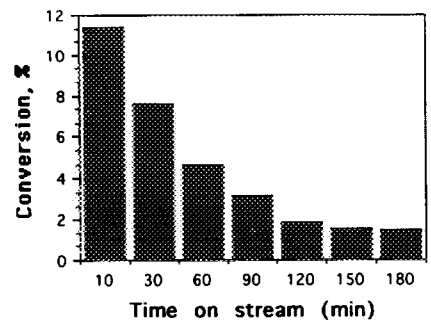

FIG. 2. Deactivation pattern of 0.88-wt% Pd/HZSM-5 in MCP conversion.

IIIb. Temperature-Programmed Oxidation (TPO)

After MCP conversion for 3 h the catalysts are characterized by TPO. Since the

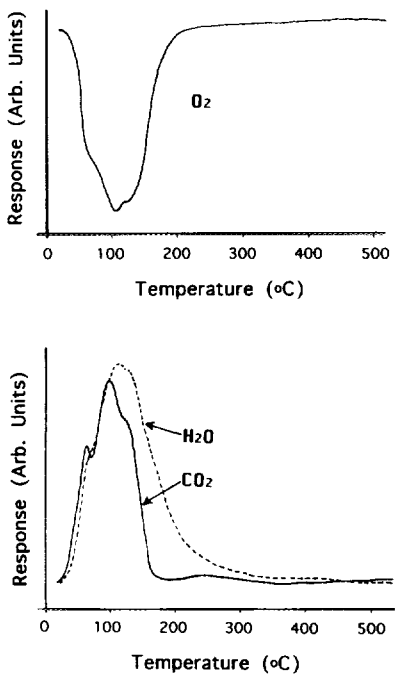

FIG. 3. Temperature programmed oxidation profiles of O_2 consumption, and CO_2 and H_2O evolution for used 0.88-wt% Pd/HZSM-5 catalyst.

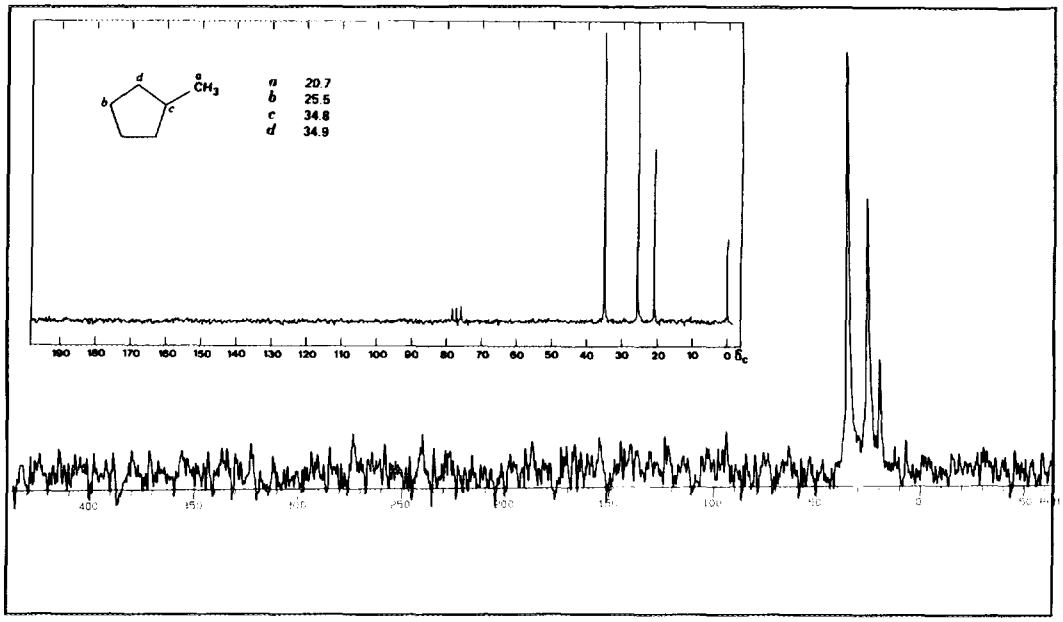

FIG. 4. ^{13}C NMR spectrum of used 0.88-wt% Pd/HZSM-5 catalyst.

TPO profiles are found very similar for catalysts of different Pd loading, we only show those obtained with 0.88 wt% Pd/HZSM-5 in Fig. 3. The consumption of O_2 and the evolution of CO_2 and H_2O mainly occurred below 200°C.

IIIc. Nuclear Magnetic Resonance (NMR)

The ^{13}C NMR spectrum of a 0.88 wt% Pd/HZSM-5 catalyst after MCP conversion of 3 h is displayed in Fig. 4. The three peaks have chemical shifts of 19.3, 25.0, and 34.6 ppm. The relative intensities are, in the same order, 25.5, 84.0, and 120.5, respectively. No unsaturated carbon atoms that would appear above 80 ppm are observed. The inset in Fig. 4 displays the ^{13}C NMR spectrum of pure MCP for comparison with the spectrum obtained for the used catalyst (*13*).

IIId. EXAFS

The EXAFS $\chi(k)$ data are shown in Fig. 5 for 0.88-wt% Pd/HZSM-5 after reduction at 250°C (a) and for the same catalyst after MCP conversion for 1 h (b). While the catalysts show a strong signal after MCP conversion, the intensity of the reduced catalysts is close to the noise level in the k-range where metal phase oscillation maximum is expected, indicating extremely low Pd-to-Pd coordination. Fourier transforms of k^2-weighted EXAFS data are presented in Figs. 6a and 6b for reduced and used catalysts respectively (phase shift uncorrected). The Fourier transforms were preformed in the k-range of 4–10 $Å^{-1}$ for the reduced catalyst and 4–14 $Å^{-1}$ for the used catalyst. Theoretical fitting to inverse Fourier transforms was performed on the first Pd–Pd shell for both the reduced and used catalysts (Fig. 7). The R-range for the inverse Fourier transform is taken between 2.0 and 3.0 for reduced catalyst; and that for used catalyst is taken between 2.0 and 2.8. The fitted coordination number, CN_{Pd}, and atomic distance (R) of nearest Pd–Pd neighbors, for reduced Pd/HZSM-5, are 1.9 and 2.73 Å, respectively. For 0.88-wt% Pd/HZSM-5 after MCP conversion the values of CN and R are 7.4 and 2.75 Å, respectively. The val-

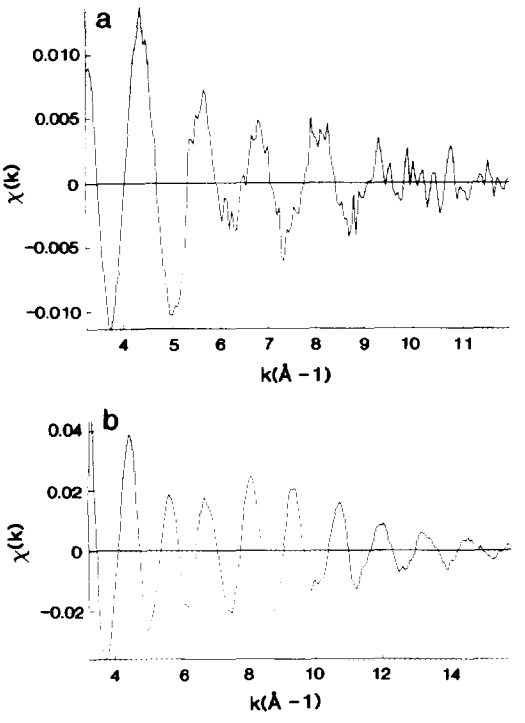

FIG. 5. EXAFS $\chi(k)$ functions of (a) Pd/HZSM-5 after calcination at 500°C for 2 h, reduction at 250°C for 20 min, and purging in He at 250°C for 20 min; and (b) same as (a) after MCP conversion at 250°C for 1 h.

ues of the Debye–Waller factor are 0.017 and 0.016 Å for the reduced catalyst and the used catalyst, respectively. The Pd–O shell of the reduced catalyst was also analysed. The fitted results show R_{Pd-O} of 2.11 Å, CN_{Pd-O} of 0.65, and Debye–Waller factor of 0.0014 Å. The error in CN typical for EXAFS is 15%; the uncertainty in R is 0.02 Å (*17*).

IIIe. Transmission Electron Microscopy (TEM)

Shown in Fig. 8 is a micrograph of 0.88-wt% Pd/HZSM-5 after reduction in H_2 at 250°C for 20 min and purging in He for 20 min. Even though zeolite lattice fringes are very clear, Pd particles in this sample are barely resolved as their size is so small that only a few appear as speckles in the micrograph. The theoretical nominal probe width of the beam is about 2 Å. Under our collection conditions the acceptable limit of error is that objects less than 4 Å of unknown periodicity may not be resolved accurately. Inspection of the exterior surface did not show any metal outside the zeolite after reduction.

After MCP conversion for 1 h, Pd particles larger than 20 Å are observed, as visible from the electron micrograph in Fig. 9. Metal particles located inside zeolites with particle sizes larger than the dimensions of the channels or cages have been reported several times before (*19–22*). It is important to note that even after reaction lattice fringes of the zeolite are still clearly resolvable, indicating that only an extremely small amount of coke, if any, is present on the catalyst.

For a sample that was reduced at 250°C

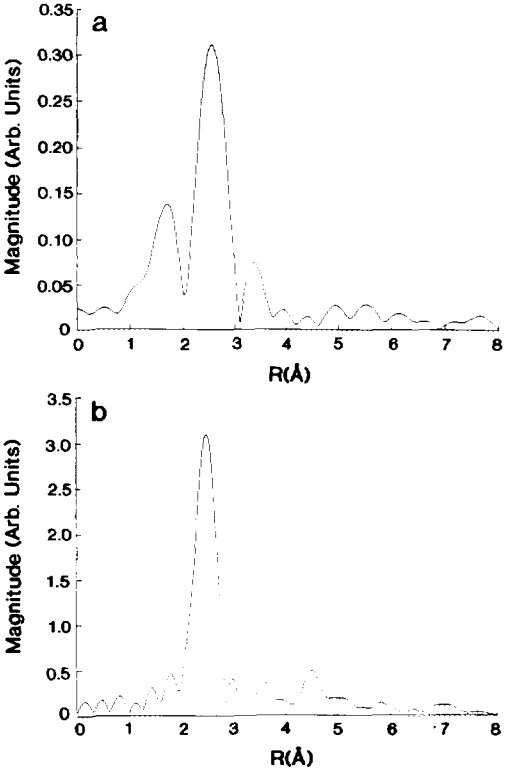

FIG. 6. Fourier transforms corresponding to (a) and (b) of Fig. 5.

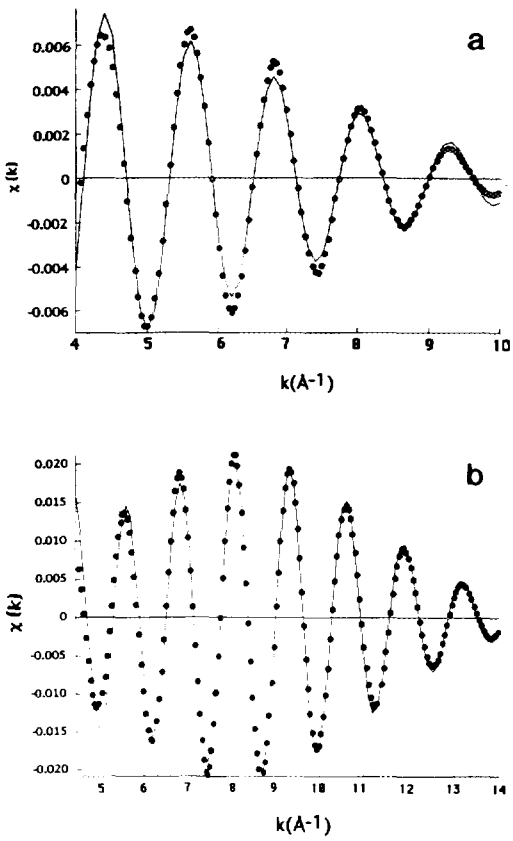

FIG. 7. EXAFS curve-fittings of nearest Pd–Pd shell for samples corresponding to (a) and (b) of Fig. 5.

for 20 min but subsequently subjected to a stream of H_2/NH_3 at the same temperature for 1 h, the electron micrograph as shown in Fig. 10 shows that Pd particles are in the order of 50 Å. Electron micrographs were also taken for a catalyst reduced at 250°C but was subsequently treated in a mixture of cyclopentane and H_2 for 1 h. The largest Pd particles in this sample are on the order of 6 Å, but many smaller ones are also discernible (Fig. 11).

IIIf. Cyclopentane H/D Exchange

Figure 12 shows the initial product distributions of the H/D exchange with cyclopentane at 100°C on a 0.88 wt% Pd/HZSM-5 catalyst. Figure 12a was obtained after reduction at 250°C in D_2, Fig. 12b after exposure of the catalysts to a D_2/CP gas mixture for 1 h at 250°C, and Fig. 12c after exposure to a D_2/MCP mixture for 1 h at 250°C.

The initial product distribution for the reduced 0.88-wt% Pd/HZSM-5 shows an apparent equilibrium pattern with a maximum at d_9. None of the usual features of H/D exchange with CP in the kinetic regime, viz., peaks at d_5 and at d_{10}, are observed in this case. After exposure to CP for 1 h at 250°C, the same catalyst displays a similar distribution pattern (Fig. 12b) with a maximum at d_9, but the d_1–d_6 fractions are higher than for the untreated catalyst. A drastically different exchange pattern is observed after exposure to MCP (Fig. 12c). The highest peak is at d_1, followed by an almost binominal decrease to d_5; then a steep drop to d_6. Qualitatively it appears that the five H atoms at the same side of the C_5 ring are exchanged against D atoms in an almost stepwise fashion; flipping over to the other side of the C_5 ring seems more difficult.

The initial rates for the disappearance of the d_0 fraction are listed in Table 1 for various catalysts. For the 0.88-wt% Pd/HZSM-5 catalyst, the rate decreased significantly after MCP treatment but the change is small after the CP treatment. For the 3.5-wt% Pd/HZSM-5 the effect on the exchange rate of exposing the catalyst to MCP is much smaller than for the low-loading sample.

The high metal load catalyst differs from the low load sample also in the initial product distribution. For the 3.5-wt% Pd/HZSM-5 catalyst the distributions before and after MCP treatment are shown in Fig. 13. For the untreated catalyst the distribution shows, again, a maximum for d_9, which might be interpreted as an equilibrium distribution for a very high extent of exchange due to long residence of the CP molecules inside the zeolite pores. After exposure to MCP the pattern is totally different: maxima at d_5 and d_{10} are symptomatic for H/D exchange of CP in the kinetic regime with a high activation energy for flipping over of the adsorbed molecule (Fig. 13b).

Reduced Pd/SiO_2 samples were used as

15A

references. The dispersion of these catalysts has been well characterized (*11*). Figure 14 shows the initial product distributions of two samples with different dispersions, one with 22.5% (Fig. 14a) and another in 65.5% (Fig. 14b). Both samples show the similar maxima for d_5 and d_{10}. The similarity with the initial product distribution obtained with the MCP treated 3.5-wt% Pd/HZSM-5 catalyst (Fig. 13b) is striking.

IV. DISCUSSION

In a previous study of MCP conversion on Pd/NaHY it was found that this catalyst loses most of its initial activity within 15 min (*12*). TPO revealed substantial deposition of coke, some associated with the metal, but the majority is ascribed to acid sites. It was assumed that coke deposition is the major cause of deactivation for that catalyst.

The present Pd/HZSM-5 catalyst also deactivates, as is apparent from Figs. 1 and 2. Deactivation is, however, much slower than with the Pd/NaHY; a steady state conversion is reached at about 2 h. Most remarkably, the 0.88-wt% Pd/HZSM-5 catalyst is more active in this stage than the 3.5-wt% Pd/HZSM-5 catalyst; coke is, apparently, *not* the major cause of deactivation. With Pd/NaHY a TPO peak at about 200°C has been identified with oke associated to Pd, and a TPO peak above 300°C with coke associated to acid sites (*12*). With the present Pd/HZSM-5 catalyst TPO maxima for O_2 consumption and CO_2 formation are small and occur at a much lower temperature near 100°C (see Fig. 3). The peak for H_2O is shifted to higher temperature due to adsorption of H_2O by the zeolite. The ^{13}C-NMR spectrum in Fig. 4 confirms that the material which is responsible for the TPO peaks is not coke, but most likely adsorbed MCP. No unsaturated hydrocarbons are detected in the NMR spectrum; reported ^{13}C-NMR chemical shifts for MCP are: 20.7 ppm for the single methyl carbon and 25.5 ppm for the two secondary carbons opposite to the tertiary carbon. The peak for the tertiary carbon at 34.8 ppm nearly coincides with that of the two neighboring secondary carbons at 34.9 ppm (*13*). Considering the line broadening and the uncertainty due to the external calibration in the present work, the intensity ratios and the chemical shifts of the ^{13}C-NMR spectrum for the used Pd/HZSM-5 catalyst are in satisfactory agreement with the corresponding literature data for MCP. The absence of unsaturated carbon from the ^{13}C-NMR spectrum supports the TPO result that coked residues are not present in the used catalyst.

Besides the TPO and the ^{13}C-NMR evidence, the TEM data also indicate the absence of substantial amounts of coke. In samples with coke the zeolite lattice fringes become obscured, as we observed on other zeolite catalysts, such as Pd/mordenite (*18*) the fringes are, however, clearly visible in the original micrographs of the present Pd/HZSM-5 catalyst after use. In fact, when rapid coking takes place for MCP conversion in acidic zeolites such as H-mordenite, the channel path was found to be blocked so that Pd agglomeration is not significant. Pd particles agglomerate, however, in Na-mordenite where less coke was detected (*18*).

In the absence of appreciable amounts of coke in used Pd/HZSM-5 we conclude that the dominant cause for the observed catalyst deactivation in the present work is agglomeration of Pd particles. In the reduced 0.88-wt% Pd/HZSM-5 sample, prior to reaction, the Pd particles are too small to be resolved by TEM (with resolution of 4 Å) and the coordination number of 1.9 for the nearest Pd–Pd shell obtained from EXAFS data shows that triatomic Pd_3 clusters pre-

FIG. 8. Electron micrograph of 0.88-wt% Pd/HZSM-5 after calcination at 500°C for 2 h, reduction at 250°C for 20 min, and purging in He at 250°C for 20 min.

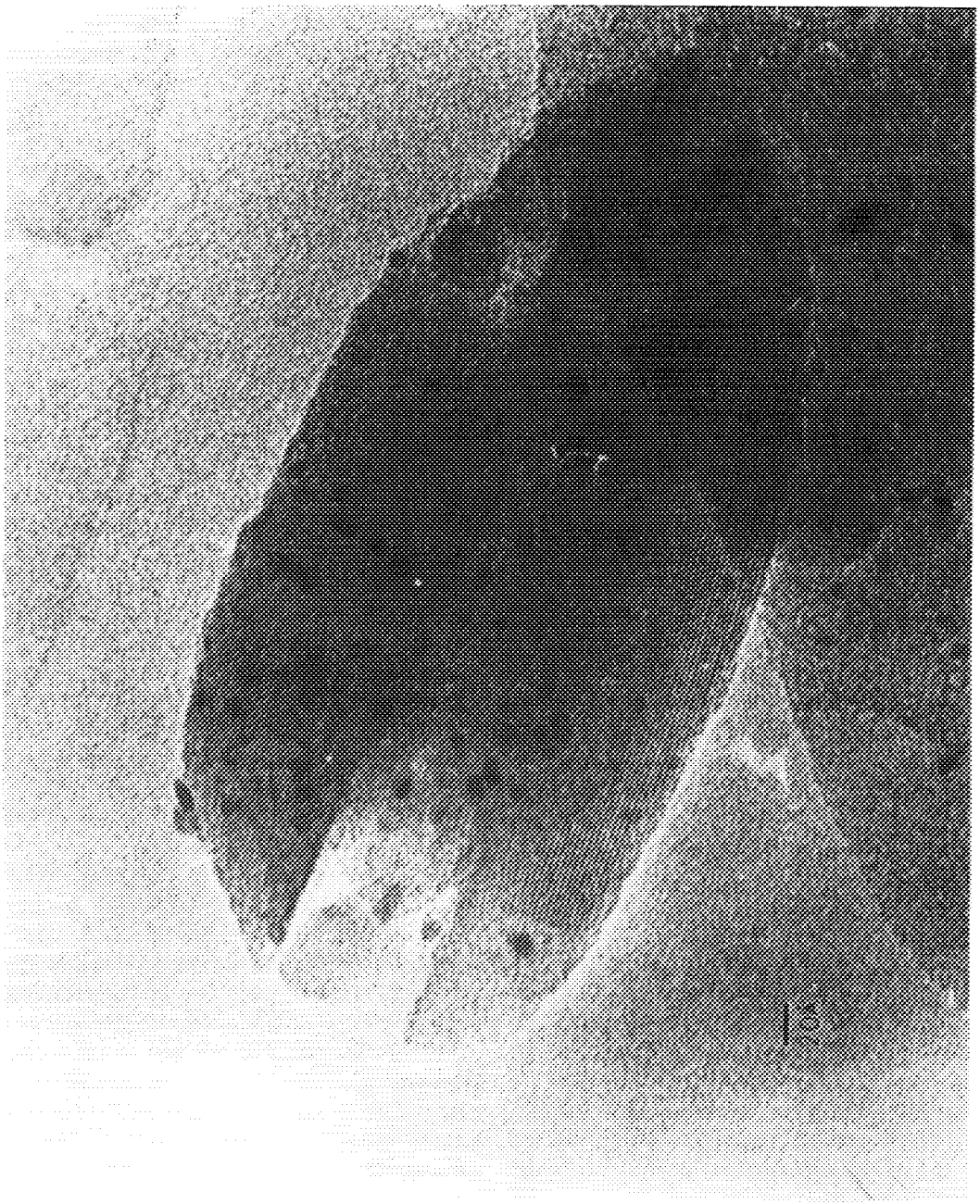

vail. Considering the error associated with CN values obtained from EXAFS in the absence of an appropriate reference for small Pd clusters, it is quite likely that the true cluster sizes will scatter around the average value of Pd_3; still the largest particles are smaller than 4–5 Å, the resolution limit of the TEM. The difference in particle size after catalysis with CP or MCP is striking. EXAFS analysius shows that after MCP catalysis the Pd–Pd coordination number has increased to 7.4; i.e., the Pd particles have become even larger than the Pd_{13} icosahedra with CN = 6, observed in other work (*1*, *2*). In accordance with these EXAFS results, the TEM micrographs show particles with diameters in the order of 20 Å. All data unambiguously prove Pd agglomeration and suggest this to be the dominant cause of catalyst deactivation. It should be pointed out that the effect of time on stream during MCP conversion is of minor importance for the agglomeration of Pd particles, because the reduced catalyst had been pretreated at 250°C for 60 min before TEM and EXAFS examination. Exposure to MCP has the most remarkable effect on the Pd agglomeration in the first 30 min on stream as shown by the conversion profile of the catalyst sample that was reduced in H_2 for 20 min before MCP reaction.

As to the mechanism of this metal agglomeration induced by MCP conversion, two possibilities are considered. First, one could assume that methylcyclopentadiene (MCPD) is produced by MCP dehydrogenation and that this molecule forms clusters with Pd in analogy to the known cyclopentadienyl Pd clusters. Such clusters might be mobile and coalesce with each other, although it is difficult so see, how triatomic Pd_3 could form a mobile cluster with one MCPD molecule, or how the larger complexes resulting from coalescence of such MCPD–Pd_3 clusters would be capable of migrating through the narrow pores of ZSM-5 of 5.5-Å diameter.

A second model focuses on the anchoring mechanism of small Pd clusters via zeolite protons (*1*, *5*, *14*). During MCP conversion, a MCP molecule will be dissociatively adsorbed on a Pd-proton adduct:

$$[Pd_n\text{–}H]^+\text{–}O_z^- + C_6H_{12} \Rightarrow [Pd_n\text{–}C_6H_{11}]^+\text{–}O_z^- + H_2.$$

In this process the Pd_n particle loses its proton anchor, it will therefore become mobile and swiftly coalesce with other Pd_n clusters. Dissociative chemisorption of MCP, in other words, destroys the proton anchor of the original metal–proton adduct. In this mechanism we have not specified the exact location of the positive charge in the $[Pd_n\text{–}C_6H_{11}]^+\text{–}O_z^-$ complex. It will presumably be shared between the Pd atoms and the C atom bonded to Pd. However, for the following discussion it may be simpler to use a terminology familiar from acid catalysis. In that field the adsorption of an olefin to a zeolite proton is often formally described as formation of a carbenium ion, although Kazansky *et al.* have shown that it would be more correct to include the O^- ion of the zeolite and call the whole complex an alkoxy group (*15*). The carbenium ion is only the transition state of the organic part of this complex. Using the same kind of simplifying terminology, we shall call the result of dissociative adsorption of a MCP molecule on the metal-proton adduct a metal–carbenium ion adduct. In this simplifying terminology we say $Pd_n\text{–}H^+\text{–}O_z^-$ when we mean $[Pd_n\text{–}H]^+\text{–}O_z^-$, and we say $Pd_n\text{–}C_6H_{11}^+\text{–}O_z^-$ when we mean $[Pd_n\text{–}C_6H_{11}]^+\text{–}O_z^-$. If the carbenium ion in this adduct is still bridging between metal cluster and cage oxide ion, the $C^+\text{–}O^-$ bond will be much weaker than the $H^+\text{–}O^-$ bond,

FIG. 9. Electron micrograph of 0.88-wt% Pd/HZSM-5 after calcination at 500°C for 2 h, reduction at 250°C for 20 min, and reaction in MCP at 250°C for 1 h.

which is another way of saying that the strong anchor has been replaced by a much weaker anchor and Pd coalescence will increase.

In the above description we have written the adduct with only one proton. This is presumably a realistic description for HZSM-5 with a Si/Al ratio of 20, but for zeolites of low Si/Al ratios such as HY, the number of proton anchors per Pd cluster will be > 1.

Two independent observations support the de-anchoring model as a major cause of Pd agglomeration. First, NH_3 molecules are known to associate with protons to form NH_4^+ ions. Our previous work showed that reduction of amminated Pd ions leads to larger Pd particles. One of the causes for this will be that the ammine ligands neutralize protons during reduction (*1*, *16*). In the present study we found that maintaining a constant NH_3 partial pressure after reduction in H_2 led to a rather dramatic Pd particle growth reaching sizes in the order of 50 Å. We consider this a direct illustration of the de-anchoring model and its drastic consequences.

The second supporting evidence is based on the comparison of MCP with CP. It is well known that the energy of tertiary carbenium ions is much lower than that of secondary carbenium ions. It follows that carbenium ion formation and thus deanchoring should be much weaker with CP, which has only secondary C atoms, than with MCP, which possesses a tertiary C atom. The strong difference in extent of metal agglomertion observed in the present study between MCP and CP supports the carbenium ion de-anchoring model. This evidence also argues against the diene model as MCP and CP should be dehydrogenated equally well to the respective cyclo-olefins.

In this discussion we have not mentioned that the products of MCP ring enlargement, in particular benzene, also change the environment of the MCP-treated catalysts in comparison to the CP-treated samples. However, closer inspection shows that this is probably not relevant for the present problem. Complexes of palladium with cyclopentene and cyclopentadiene or their methylated homologs are known to be much more stable than complexes with aromatics. If any of these complexes were responsible for the coalescence of Pd clusters, CP and MCP would be expected to be very similar. The observed dramatic difference between CP and MCP is, therefore, most likely due to the presence of the tertiary C atom in MCP.

The importance of the tertiary C atom in metal agglomeration is also illustrated by the marked differences between exposure to CP and to MCP, as probed with the isotope exchange of CP. As the present data show, exposure to MCP at 250°C results in a significant change in the initial product distribution. This indicates, again, a rather drastic change in the morphology as well as the environment of the metal crystallite. The dominant stepwise exchange process and the steric restriction for the diffusion of CP molecules in the MCP treated 0.88-wt% Pd/HZSM-5 catalyst suggest that the active metal sites are within the ZSM-5 zeolite channel. The exchange process is strongly influenced by the small pore size of the ZSM-5 channel. The significant drop in the initial rate of the disappearance of d_0 is probably due to partial blocking and decrease in the number of effective metal sites as a result of the metal agglomeration due to MCP treatment. The sudden drop between d_5 and d_6 is indicative of the desorption of CP molecules after one side of the C_5 ring is fully deuterated inside zeolite channel. In contrast to this, exposure to CP at the same

FIG. 10. Electron micrograph of 0.88-wt% Pd/HZSM-5 after calcination at 500°C for 2 h, reduction at 250°C for 20 min, and exposed to H_2/NH_3 mixture at 250°C for 1 h.

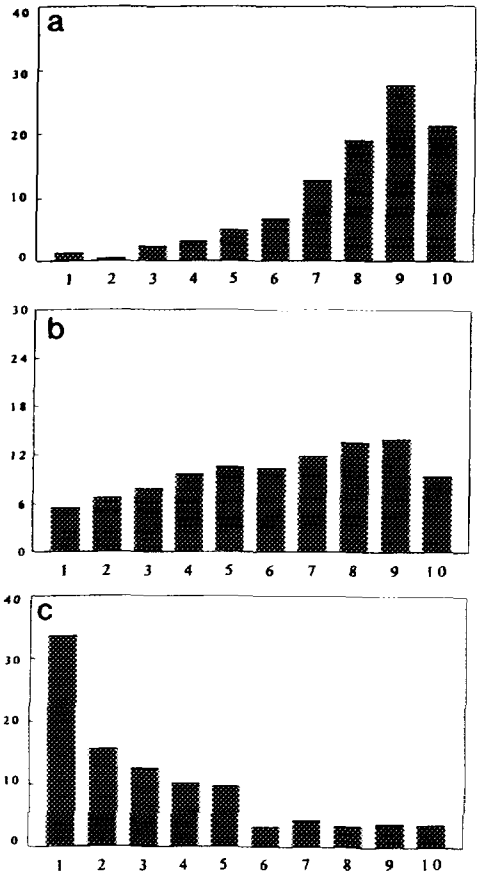

FIG. 12. Initial product distribution in CP H/D exchange with 0.88-wt% Pd/HZSM-5 (a) after calcination at 250°C and reduction at 250°C for 20 min; (b) same as (a) after CP treatment at 250°C for 1 h; and (C) same as (a) after MCP treatment at 250°C for 1 h.

temperature does not induce a significant change in the initial product distribution and in the initial rate of d_0 disappearance. The similarity of the initial product distribution between the high-Pd-loading catalyst and Pd/SiO_2 suggests that a large portion of the Pd particles in the high-Pd-loading catalyst after agglomeration in MCP treatment is on the external surface of the zeolite crystallites, as may also be inferred from the TEM images which show metal particles at the grain boundaries of the zeolite crystal. A similar criterion for determining the migra-

TABLE 1

Initial Rate of Disappearance of Undeuterated CP (d_0)

Pd loading (wt%), treatment	Rate (%/min-15 mg)
0.88, Reduced	41.4
0.88, CP treated	35.5
0.88, MCP treated	9.1
3.5, Reduced	52.3
3.5, MCP treated	48.8

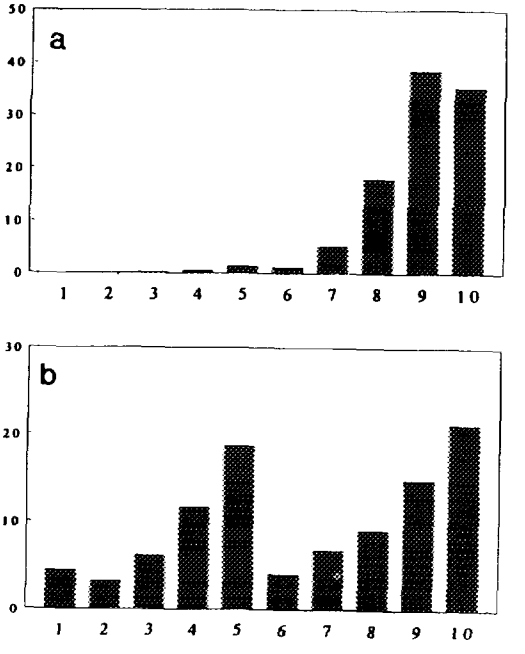

FIG. 13. Initial product distribution in CP H/D exchange with 3.5-wt% Pd/HZSM-5 after (a) calcination at 250°C and reduction at 250°C for 20 min; and (b) same as (a) after MCP treatment at 250°C for 1 h.

FIG. 11. Electron micrograph of 0.88-wt% Pd/HZSM-5 after calcination at 500°C for 2 h, reduction at 250°C for 20 min, and reaction in CP at 250°C for 1 h. The particle distribution involves a minority such as "A" in 6–10 Å, and a majority of "B" in less than 6 Å.

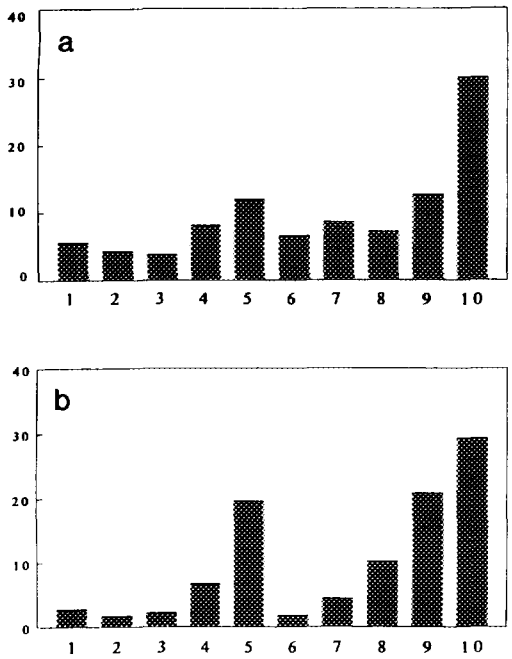

FIG. 14. Initial product distribution of CP H/D exchange on Pd/SiO_2 with Pd dispersions of (a) 22.5% and (b) 65.5%.

tion of particles to the external surface of zeolite has been reported by Pan *et al. (23)*. In contrast, for the 0.88-wt% Pd/HZSM-5 after MCP treatment Pd particles are mainly occluded inside the zeolite, possibly by local collapse of the zeolite lattice.

V. CONCLUSIONS

The strong agglomeration of Pd in H-ZSM5 after exposure to reacting MCP is caused by *de-anchoring*, via replacement of the original proton in the palladium–proton adduct by, formally, a carbenium ion. Similar de-anchoring by exposure to ammonia confirms this interpretation. The much lower extent of metal agglomeration induced by CP is attributed to the lower tendency of this molecule, in comparison to MCP, to form carbenium ions.

ACKNOWLEDGMENTS

The authors thank Professor E. A. Stern of University of Washington for kindly donating his EXAFS package. Financial support by the National Science Foundation, Contract CTS-8911184/02, is gratefully acknowledged. We thank Professor Vinayak Dravid for his kind permission to make TEM micrographs in his laboratory, and Dr. Xiwei Lin for his help with this technique.

REFERENCES

1. Zhang, Z. Chen, H., and Sachtler, W. M. H., *J. Chem. Soc. Faraday Trans.* **87,** 1413 (1991).
2. Zhang, Z., Chen, H., Sheu, L. L., and Sachtler, W. M. H., *J. Catal.* **127,** 213 (1991).
3. Zhang, Z., Wong, T. T., and Sachtler, W. M. H., *J. Catal.* **128,** 13 (1991).
4. Zhang, Z., and Sachtler, W. M. H., *J. Mol. Catal.* **67,** 349 (1991).
5. Xu, L., Zhang, Z., and Sachtler, W. M. H., *J. Chem. Soc. Faraday Trans.*, **88,** 2291, (1992).
6. Stakheev, A. Yu., and Sachtler, W. M. H., *J. Chem. Soc. Faraday Trans.* **87,** 3703 (1991).
7. Homeyer, S. T., Karpiński, Z., and Sachtler, W. M. H., *Recl. Trav. Chim. Pays-Bas* **109,** 81 (1990).
8. Augustine, S. M., and Sachtler, W. M. H., *J. Catal.* **106,** 417 (1987).
9. van Broekhoven, E. H., and Ponec, V., *J. Mol. Catal.* **25,** 109 (1984).
10. Kemball, C., *Adv. Catal.* **11,** 223 (1959).
11. Nandi, R. K., Georgopoulos, P., Cohen, J. B., Butt, J. B., Burwell, R. L., Jr., and Bilderback, D. H., *J. Catal.* **77,** 421 (1982).
12. Homeyer, S. T., Karpiński, Z., and Sachtler, W. M. H., *J. Catal.* **123,** 60 (1990).
13. Johnson, L. F., and Jankowski, W. C., "Carbon-13 NMR Spectra," Wiley, New York, 1972.
14. Sachtler, W. M. H., *Catal. Today* **15,** 419 (1992).
15. Kazansky, V. B., *Acc. Chem. Res.* **24,** 379 (1991).
16. Homeyer, S. T., and Sachtler, W. M. H., *J. Catal.* **117,** 91 (1989).
17. Stern, E. A., *in* "X-ray Absorption: Principles, Applications, Techniques of EXAFS, SEXAFS, and XANES" (D. C. Koningsberger and R. Prins, Eds.), Chap. 1, Wiley, New York, 1987.
18. Lerner, B., Zhang, Z., and Sachtler, W. M. H., *J. Chem. Soc. Faraday Trans.*, submitted.
19. Jaeger, N. I., Jourdan, A. L., Schulz-Ekloff, G., and Svensson, A., *in* "Structure and Reactivity of Surfaces, (C. Morterra, A. Zecchina, and G. Costa, Eds.), p. 503, Elsevier, Amsterdam, 1989.
20. Jaeger, N. I., Rathousky, J., Schulz-Ekloff, G., Svensson, A., and Zukal, A., *in* "Zeolites: Facts Figures, Future" (P. A. Jacobs and R. A. van Santen, Eds.), p. 1005, Elsevier, Amsterdam, 1989.
21. Wank, M., Schulz-Ekloff, G., and Jaeger, N. I., *Catal. Today* **8,** 467 (1991).
22. Schulz-Ekloff, G., Wright, D., and Grunze, M., *Zeolites* **2,** 70 (1982).
23. Pan, M., Cowley, J. M., and Chan, I. Y., *Catal. Lett.* **5,** 1 (1990).